33RD CONGRESS
OF THE INTERNATIONAL COUNCIL
OF THE AERONAUTICAL SCIENCES
STOCKHOLM, SWEDEN, 4-9 SEPTEMBER, 2022

ICAS 2022 SWEDEN

AEROELASTIC ANALYSIS OF HIGH ASPECT RATIO AND STRUT-BRACED WINGS

Yoann LE LAMER[1], Joseph MORLIER[2], Emmanuel BENARD[1] & Ping HE[3]

[1]ISAE-SUPAERO, Université de Toulouse, Toulouse, France
[2]ICA, Université de Toulouse, ISAE-SUPAERO, MINES ALBI, UPS, INSA, CNRS, Toulouse, France
[3]Iowa State University, Ames, USA

Abstract

Increasing the aspect ratio of transonic aircraft wings represent a promising path to allow aviation to reduce its carbon footprint. The objective of this study is to develop sufficiently accurate aero-structural models in order to fully exploit High Aspect Ratio (HAR) wings drag reduction and performance improvements potential at preliminary design stage. The use of a multifidelity approach makes it possible to reduce computational costs by mainly resorting to low-fidelity computations and only running high-fidelity computations when necessary. The first step is to develop high and low fidelity models to perform static aeroelastic analysis on the NASA CRM wing. These models will be used as a baseline to be compared with other configurations of interest. Afterwards, models are developed for a modified version of the CRM wing with a higher aspect ratio, and static aeroelastic analysis are carried out. Finally, a Strut-Braced Wing (SBW) configuration is studied to evaluate its mass reduction potential, in addition to the drag reduction provided by the increased aspect ratio. These aero-structural models are implemented within an in-house aeroelastic analysis and optimization framework. This works focuses on aeroelastic analysis for now, but is to be extended to aeroelastic optimization, using a multifidelity approach.

Keywords: High Aspect Ratio (HAR) wings, Strut-Braced wings (SBW), Aeroelasticity, Multidisciplinary Design Analysis (MDA)

1. Introduction

High aspect ratio (HAR) configurations have a great potential for reducing induced drag, and thus fuel consumption and aircraft carbon footprint [1]. Multidisciplinary design optimization (MDO), and in particular aerostructural optimization is necessary in order to make the most of these configurations [2]. Because of high computational costs [3], and in an effort to effectively assess the performance of multiple configurations, models need to be developed for carrying out preliminary design studies.

The issue of computational costs [3] is critical when it comes to aerostructural studies. This can be dealt with by resorting to surrogate models to approximate a system [4], be it for CFD or finite-elements analysis (FEA), using a certain number of samples. Multifidelity can also be an promising strategy to mitigate computational costs. Indeed, using such a method, surrogate models are trained using models with different levels of fidelity, and thus accuracy and computational costs. An algorithm helps find a balance between computation time and physical accuracy.

In this work we use an aeroelastic analysis and optimization framework developed by [5], the aerostructure package [6], which is implemented within the OpenMDAO framework [7].

The final goal of this study is to use aerostructural models of both high and low fidelity to apply a multifidelity approach in order to assess the performance of several configurations of interest in an efficient way. This paper will include the development of high and low fidelity aeroelastic models for different configurations. Also, high and low fidelity aeroelastic analysis are run and results compared.

In section 2.the different configurations of interest are presented along with their associated baseline configurations to be used for comparison. Section 3. presents the general framework that is used to perform aerostructural analysis. The different high and low fidelity models are presented and the way they are generated is detailed. Finally, validation and application cases results are presented in section 4. Conclusions and future work are listed in section 5.

2. Targeted configurations

The objective of this work is to study different configurations to assess potential performance improvements.

The first goal is to study the effects of increasing wing aspect ratio. To this purpose we chose to focus on the uCRM-13.5 model developed in [8]. This model corresponds to a modified version of the NASA CRM model, with an aspect ratio increased by 50%. Main geometrical dimensions are summarized in table 1. Also, uCRM-9.0 geometry will be used as a baseline in order to assess the benefits of increasing the aspect ratio, particularly in term of induced drag reduction. This model corresponds to the undeformed version of NASA Common Research Model (CRM) [9]. The so developed models are validated using data provided in [8], for both uCRM-9.0 and uCRM-13.5. Figure 1 presents the geometry of the NASA CRM wing.

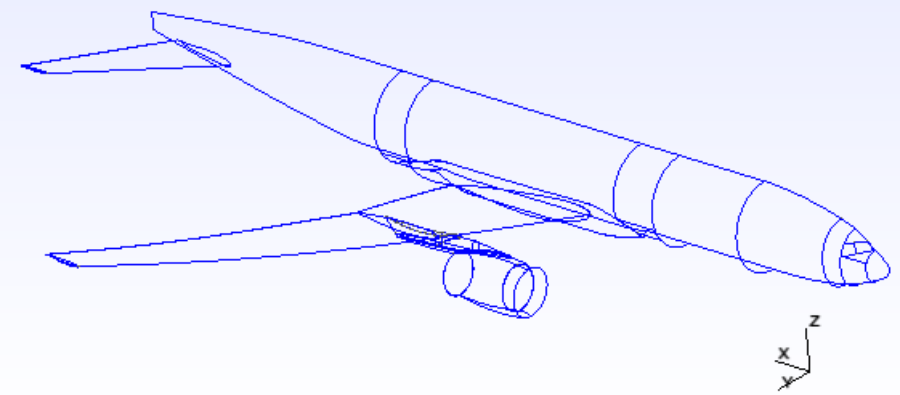

Figure 1 – Geometry of the NASA Common Research Model (CRM).

The second goal is to study the effects of adding a strut to a high aspect ratio wing, particularly in terms of potential mass reduction. To this purpose we chose to generate a SBW version of the uCRM-13.5 configuration. Main geometrical dimensions are the same than uCRM-13.5 (see table 1) except for the strut. The strut-wing junction is positioned at 42% of half-span and at 50% of the corresponding chord.

3. Methodology

3.1 Aerostructural framework implementation

The aeroelastic analysis and optimization framework used in this study, developed by [5], is written in Python language and makes use of the OpenMDAO platform that is well suited for MDAO problems. This framework is able to solve both static and dynamic aeroelasticity problems. The way it works is presented in figure 2, each block (green boxes) corresponds to a specific component. The other boxes are used for linking the components together, feeding inputs from different outputs. Here two main disciplines run within the framework. First, the aerodynamic problem is solved either with DAFOAM or AVL depending on the chosen level of fidelity. Then, solving the structural problem is done by running MSC Natran finite-element analysis (FEA), either for a 1D beam model or a 3D wingbox model depending on the desired level of fidelity.

Name	uCRM-9.0	uCRM-13.5
Planform area [m^2]	383.74	384.05
Span [m]	58.76	72.00
MAC [m]	7.01	5.36
Aspect ratio	9.0	13.5
Taper ratio	0.275	0.250
1/4 Chord sweep [deg]	35.0	35.0
Cruise Mach	0.85	0.85

Table 1 – Main geometrical parameters of targeted configurations.

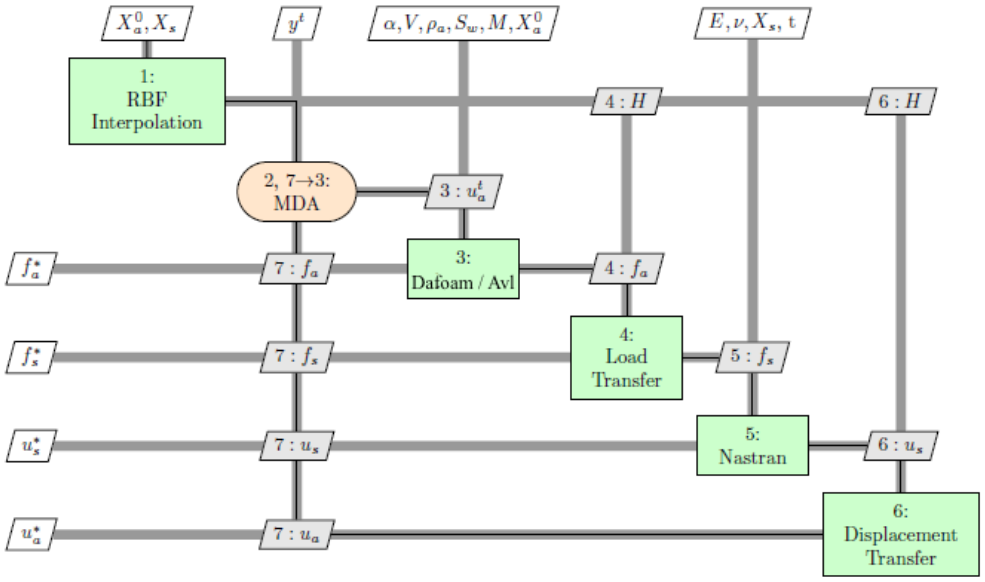

Figure 2 – XDSM diagram of the static aeroelastic OpenMDAO HF/LF solver.

A mesh interpolation scheme that depends on the selected models is used for transferring loads from the aerodynamic solver to the structural mesh, and displacements from the structural solver to the aerodynamic mesh. In this work, low-fidelity computations are performed using both LF structural and aerodynamic models. Likewise, HF computations are carried out with both HF models.

The fluid-structure interaction problem is solved using an iterative partitioned approach. This process runs iteratively until convergence is achieved, based on selected quantities of interest.

3.2 Model description and generation workflow

For both high and low fidelity (HF and LF) simulations, only a half wing is considered, because a symmetry condition is applied in order to reduce computation time.

3.2.1 High-fidelity (HF) computations

In order to perform HF aerodynamic computations, the DAFOAM [10] solver is used to run CFD. For now, this aerodynamic code is used to solve steady Navier-Stokes equations. Airflow is considered viscous, turbulent and compressible. For generating the CFD mesh, a surface mesh is first created as a .stl file using OpenVSP [11], then the unstructured volume mesh is generated using SnappyHexMesh, which is an OpenFOAM built-in meshing tool [12]. The workflow to be followed in order to obtain HF aerodynamic loads is illustrated in figure 3.

The objective being to perform aerostructural analysis, the previously described aerodynamic solver needs to be coupled with a finite-elements analysis (FEA) solver, here the MSC Nastran software

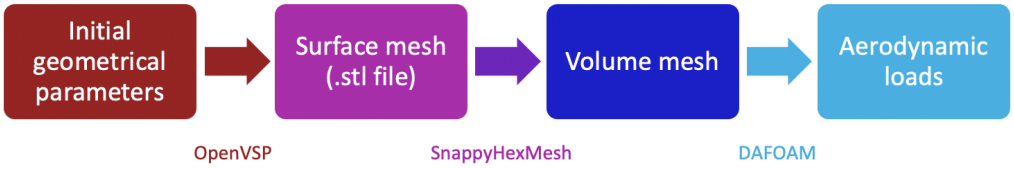

Figure 3 – HF aerodynamic computational workflow.

[13] is used. A three-dimensional wingbox finite-elements model (FEM) is generated as a BDF file. This wingbox shell-model breaks down into several components, upper and lower skin, ribs, spars and stiffeners. Skin, ribs and spars are represented using shell elements (CQUAD4), and stiffeners are represented using beam elements (CBAR). A Python module has been specifically developed to generate this model based on wing geometrical and material properties inputs. An example of a so developed FE mesh for the CRM wing is presented in figure 4.

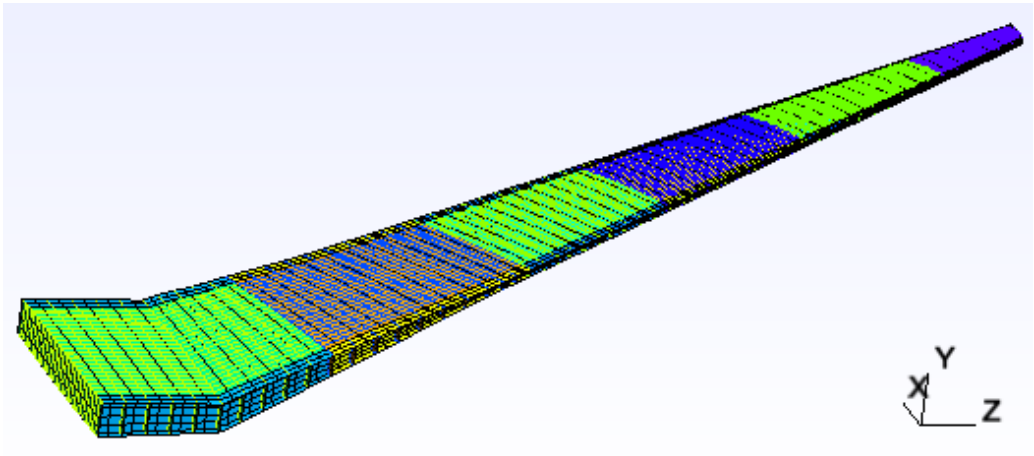

Figure 4 – CRM structural FE model generated using dedicated module.

The wingbox structural models used in this work for uCRM-9.0 and uCRM-13.5 have been validated by comparing with results from [8]. Interpolation between aerodynamic and structural meshes is used to transfer loads and displacements. This is performed thanks to radial basis functions (RBF), using Thin Plate Splines (TPS) approximation developed in [14].

For now only linear FEA has been considered and tested, but the possibility to easily switch from a linear to a non-linear structural solver is also implemented for later use.

3.2.2 Low-fidelity (LF) computations

In order to perform LF aerodynamic computations, the AVL code [15] is used to carry out VLM (Vortex Lattice Method) computations, the corresponding model is generated through a dedicated Python module based on wing geometrical properties inputs. The model is defined through a certain number of control points, and associated chords, and twists. The workflow to be followed in order to obtain LF aerodynamic loads is presented in figure 5.

This VLM solver is also coupled to MSC Nastran [13]. Contrary to HF computations, a one-dimensional finite-elements model (FEM) is generated as a BDF file. The wing is split into a certain number of

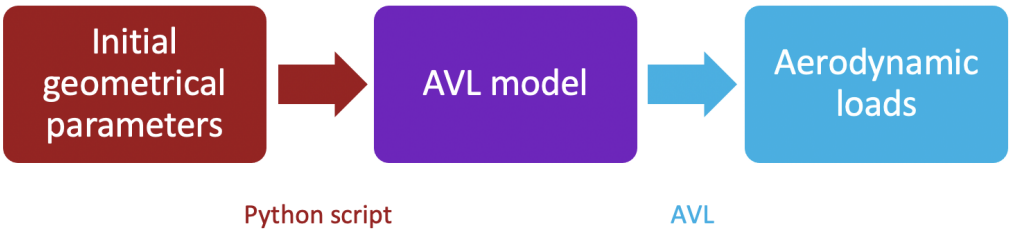

Figure 5 – LF aerodynamic computational workflow.

beam elements (CBAR). Another specific Python module has been developed to generate this model based on the wing geometrical and material properties.

The beam elements used in this model correspond to a rectangular beam section. Geometrical parameters, namely height, length, skin and spar thicknesses are the parameters, are used as inputs, and corresponding stiffness properties are computed thanks to the script.

4. Validation and application cases

The material considered in this study for structural models components is Aluminum alloy 7000 series. Its mechanical properties are presented in 2. Structural elements are sized to ensure that their maximum Von Mises stress is inferior to the material yield stress 2 with a safety factor of 1.5, corresponding to 280 MPa. Computations are performed for both 1g and 2.5g load cases. The 2.5g extreme load case is the one being used for structural sizing. To be more specific, the 2.5g load case corresponds to the cruise condition where lift balances 2.5 times aircraft mass.

Parameter	Value
Density [kg/m3]	2780
Young's Modulus [MPa]	73100
Poisson Ratio	0.33
Yield Stress [MPa]	420

Table 2 – Material properties.

4.1 Model validation: undeflected CRM wing

First of all, we focus on the uCRM-9.0 configuration, that corresponds to our baseline for this study. The previously described MDA framework is applied to both LF and HF cases, in order to validate it against available validation data. Corresponding structural and aerodynamic models are generated based on model chord and twist distributions, and wingpress geometry developed and presented in [8]. Flight conditions for each load case are described in 3.

Results of LF computations are summarized in 4. It shows that wing mass is underestimated, by approximately -20% with regard to validation. Conversely, wingtip displacement is overestimated by almost 20%.

As expected, high-fidelity results presented in 5 are closer to validation data than low-fidelity results. Wingtip displacement is still overestimated, but is now around 5%. Mass is understimated by approximately -8%.

Load case	1 g	2.5 g
CL (half-wing)	0.5	0.5*2.5
Mach number	0.85	0.85
Flight altitude [ft]	37,000	37,000

Table 3 – Flight conditions for each load case for MDA on uCRM-9.0 geometry.

Load case	1 g	2.5 g
AoA [deg.]	1.5	6.33
Estimated CDi [drag counts]	98	613
Oswald coefficient	0.89	0.71
Wingtip displacement [m]	3.10	5.84
Reference wingtip displacement [m]	2.59	-
Deviation [%]	19.7	-
Mass [kg]	9510	9510
Reference mass [kg]	11,959	11,959
Deviation [%]	-20.1	-20.1
Computation time [s]	64	122

Table 4 – Results of LF aeroelastic MDA for uCRM-9.0 geometry (reference data from [8]).

Load case	1 g	2.5 g
AoA [deg.]	2.52	8.47
Estimated CDi [drag counts]	89	560
Wingtip displacement [m]	2.73	5.03
Reference wingtip displacement [m]	2.59	-
Deviation [%]	5.4	-
Mass [kg]	11,002	11,002
Reference mass [kg]	11,959	11,959
Deviation [%]	-8.1	-8.1
Computation time [s]	1014	1352

Table 5 – Results of HF aeroelastic MDA for uCRM-9.0 geometry (reference data from [8]).

4.2 Application to a HAR configuration

In this subsection, the same method is applied to uCRM-13.5 high aspect ratio configuration to estimate wing mass and examine how induced drag is affected by an increase in aspect ratio. As for uCRM-9.0, structural and aerodynamic models are generated based on model chord and twist distributions, and wingpress geometry developed and presented in [8]. Flight conditions for each load case are described in 6.

Results of LF computations are summarized in 7. Mass evaluation shows the same trend than for the CRM wing, being a mass underestimation, here by approximately -12%. Unlike the CRM wing, results show that wingtip displacement is unexpectedly underestimated, by almost -30%.

Besides, HF results presented in 8 are closer to validation data than LF results. Mass and wingtip displacements are still understimated, by around -5% and -14% respectively.

As expected, it appears from 4 and 7, that induced drag is lower for the uCRM-13.5 high-aspect ratio configuration than for the reference uCRM-9.0 reference configuration. Induced drag reduction could be higher as aerodynamic efficiency (e.g. Oswald factor) is lower in the HAR case, probably because

Load case	1 g	2.5 g
CL (half-wing)	0.55	0.55*2.5
Mach number	0.85	0.85
Flight altitude [ft]	37,000	37,000

Table 6 – Flight conditions for each load case for MDA on uCRM-13.5 and SBW uCRM-13.5 geometries.

Load case	1 g	2.5 g
AoA [deg.]	1.81	9.86
Estimated CDi [drag counts]	91	610
Oswald coefficient	0.76	0.74
Wingtip displacement [m]	4.24	10.27
Reference wingtip displacement [m]	6.05	-
Deviation [%]	-29.9	-
Mass [kg]	13,303	13,303
Reference mass [kg]	15,016	15,016
Deviation [%]	-11.4	-11.4
Computation time [s]	82	176

Table 7 – Results of LF aeroelastic MDA for uCRM-13.5 geometry (reference data from [8]).

aerodynamic shape is not optimized or because of discretization that comes with VLM computations.

Load case	1 g	2.5 g
AoA [deg.]	2.67	9.92
Estimated CDi [drag counts]	81	512
Wingtip displacement [m]	5.19	11.52
Reference wingtip displacement [m]	6.05	-
Deviation [%]	-14.2	-
Mass [kg]	14,165	14,165
Reference mass [kg]	15,016	15,016
Deviation [%]	-5.7	-5.7
Computation time [s]	1152	1981

Table 8 – Results of HF aeroelastic MDA for uCRM-13.5 geometry (reference data from [8]).

4.3 Application to a HAR SBW configuration

Finally, we will evaluate mass reduction that can be be obtained when adding a strut to a HAR configuration, here the uCRM-13.5 configuration.

In this part where we add the strut, we decided as a first approximation not to consider the strut in the aerodynamic mesh as its contribution is rather to friction drag than to lift. It is considered to be designed as a non-lifting surface in this example. The strut considered in this paper has a rectangular shape, with two parameters for each section, namely height (length is twice the height) and panel thickness. Therefore, only structural models had to be regenerated, and aerodynamic models remains unchanged. Flight conditions for each load case are described in 6.

Results of LF and HF computations are summarized in 9 and 10. Wingtip displacement is reduced

Load case	1 g	2.5 g
AoA [deg.]	1.41	8.67
Estimated CDi [drag counts]	91	585
Oswald coefficient	0.77	0.77
Wingtip displacement [m]	3.67	9.07
Mass [kg]	10,983	10,983
Computation time [s]	98	172

Table 9 – Results of LF aeroelastic MDA for SBW uCRM-13.5 geometry.

by -13% with the LF computations and by -9% with the HF computations. That is consistent with the strut reducing wing flexibility. It can also be observed that the mass is significantly reduced with regard to the HAR configuration analyzed in the previous subsection. Indeed, the mass reduction is of -17.4% with the LF analysis and -18.8% with the HF analysis. This confirms the mass reduction potential of a SBW configuration.

Load case	1 g	2.5 g
AoA [deg.]	2.70	9.65
Estimated CDi [drag counts]	79	514
Wingtip displacement [m]	4.72	10.53
Mass [kg]	11,502	11,502
Computation time [s]	1100	2104

Table 10 – Results of HF aeroelastic MDA for SBW uCRM-13.5 geometry.

5. Conclusions and future work

5.1 Main results

This study allowed to evaluate aeroelastic analysis capacities of our in-house framework against reference data, from [8], for the undeflected NASA CRM (uCRM-9.0) wing as well as for its HAR version (uCRM-13.5). Comparisons with the reference values for both configurations are presented in 6 and 8. Also, we have confirmed the expected result that induced drag is actually reduced when increasing the aspect ratio as illustrated by 7. Finally, the performed analysis have illustrated the mass reduction potential of SBW configurations.

5.2 Future work

In order to maximize the benefits of the previously studied configurations, it would be necessary to perform aeroelastic optimization and compare quantities of interest between the so obtained optimized geometries. To this purpose, we are planning to use a multifidelity optimization approach that would allow us to mitigate computation costs. It seems to be a promising approach as previous analysis show that LF simulations run more than 10 times faster than HF simulations. The first step could be to use a strategy close to the one we described in [16], and later we would use MFEGO methodology as presented in [17]. That would require to test and run HF and LF optimizations separately using our in-house framework.

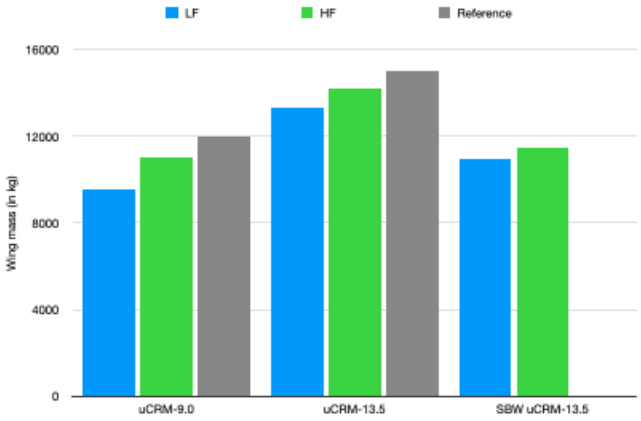

Figure 6 – Synthesis of wing mass values for each configuration of interest.

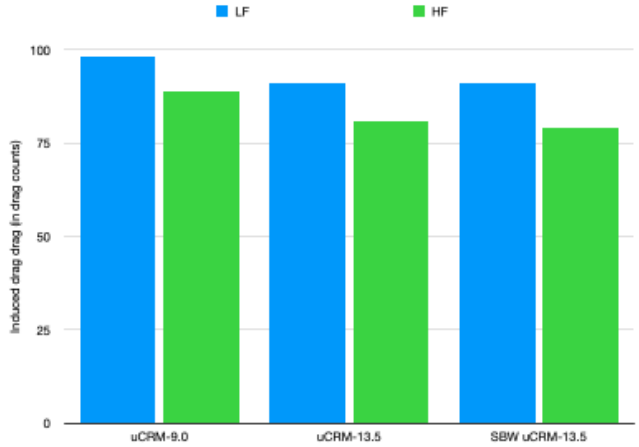

Figure 7 – Synthesis of induced drag values for each configuration of interest.

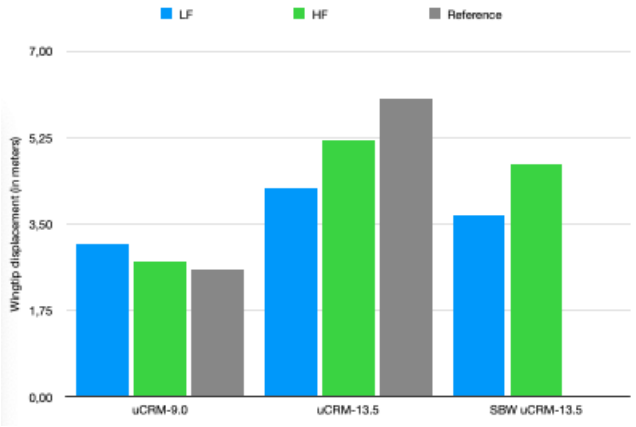

Figure 8 – Synthesis of wingtip displacement values for each configuration of interest.

6. Contact Author Email Address

mailto: yoann.le-lamer@isae-supaero.fr

7. Copyright Statement

References

[1] Brooks, T., Kennedy, G., and Martins, J., "High-fidelity Multipoint Aerostructural Optimization of a High Aspect Ratio Tow-steered Composite Wing," 2017. https://doi.org/10.2514/6.2017-1350.

[2] Kenway, G. K. W., and Martins, J. R. R. A., "Multipoint High-Fidelity Aerostructural Optimization of a Transport Aircraft Configuration," *Journal of Aircraft*, Vol. 51, No. 1, 2014, pp. 144–160. https://doi.org/10.2514/1.C032150, URL https://arc-aiaa-org.rev-doc.isae.fr/doi/10.2514/1.C032150, publisher: American Institute of Aeronautics and Astronautics.

[3] Kennedy, M. C., and O'Hagan, A., "Predicting the Output from a Complex Computer Code When Fast Approximations Are Available," *Biometrika*, Vol. 87, No. 1, 2000, pp. 1–13.

[4] Jones, D. R., "A Taxonomy of Global Optimization Methods Based on Response Surfaces," *Journal of Global Optimization*, Vol. 21, No. 4, 2001, pp. 345–383.

[5] Mas-Colomer, J., "Aeroelastic Similarity of a Flight Demonstrator via Multidisciplinary Optimization," Ph.D. thesis, 12 2018.

[6] Colomer, J. M., "Aerostructure package," , 2019. URL https://github.com/mid2SUPAERO/aerostructures.

[7] Gray, J. S., Hwang, J. T., Martins, J. R. R. A., Moore, K. T., and Naylor, B. A., "OpenMDAO: an open-source framework for multidisciplinary design, analysis, and optimization," 2019.

[8] Brooks, T. R., Kenway, G. K., and Martins, J. R. R. A., "Undeflected Common Research Model (uCRM): An Aerostructural Model for the Study of High Aspect Ratio Transport Aircraft Wings," *35th AIAA Applied Aerodynamics Conference*, American Institute of Aeronautics and Astronautics, ???? https://doi.org/10.2514/6.2017-4456.

[9] NASA, "NASA Common Research Model," , 2017. URL https://commonresearchmodel.larc.nasa.gov/.

[10] He, P., Mader, C., Martins, J., and Maki, K., "DAFoam: An Open-Source Adjoint Framework for Multidisciplinary Design Optimization with OpenFOAM," *AIAA Journal*, 2019, p. 2019. https://doi.org/10.2514/1.j058853.

[11] Fredericks, W., Antcliff, K., Costa, G., Deshpande, N., Moore, M., San, E., and Snyder, A., "Aircraft Conceptual Design Using Vehicle Sketch Pad," 2010. https://doi.org/10.2514/6.2010-658.

[12] Weller, H., Tabor, G., Jasak, H., and Fureby, C., "A Tensorial Approach to Computational Continuum Mechanics Using Object Orientated Techniques," *Computers in Physics*, Vol. 12, 1998, pp. 620–631. https://doi.org/10.1063/1.168744.

[13] Lahey, R. S., Miller, M. P., and Reymond, M., "MSC/NASTRAN reference manual, version 68," *The MacNeal-Schwendler Corporation*, 1994.

[14] Rendall, T. C. S., and Allen, C. B., "Unified fluid–structure interpolation and mesh motion using radial basis functions," *International Journal for Numerical Methods in Engineering*, Vol. 74, No. 10, 2008, pp. 1519–1559. https://doi.org/https://doi.org/10.1002/nme.2219, URL https://onlinelibrary.wiley.com/doi/abs/10.1002/nme.2219.

[15] Drela, M., and Youngren, H., "AVL overview," , 2013. URL http://web.mit.edu/drela/Public/web/avl/.

[16] Lamer, Y. L., Quaglia, G., Bénard, E., and Morlier, J., "Multifidelity aeroelastic optimization applied to har wing," *Aerobest 2021*, Virtual event, PT, 2021, pp. 454–472. URL https://oatao.univ-toulouse.fr/28740/.

[17] Bartoli, N., Meliani, M., Morlier, J., Lefebvre, T., Bouhlel, M.-A., and Martins, J., *Multi-fidelity efficient global optimization: Methodology and application to airfoil shape design*, 2019. https://doi.org/10.2514/6.2019-3236, URL https://arc.aiaa.org/doi/abs/10.2514/6.2019-3236.